

https://dspace.org/

Creation of a benchmark sample to facilitate gap etching analysis of pre-payment meter surge arresters removed from the field

Koert, Arend Jan

2008-08-08T11:54:39Z
http://hdl.handle.net/10539/5318

Downloaded from a DSpace repository. https://dspace.org/

5 CREATING AND ANALYSING THE BENCHMARK SAMPLE

Chapter 4 describes the design and construction of six resistive inductor components. These components yield only two[1] waveforms (8/20 μs and 4/70 μs) out of the four waveforms required as per the test space (refer to Chapter 3), and hence were used to create and analyse a reduced benchmark sample prior to possible further resistive inductor design and construction.

5.1 Quantifying I vs. V_s per Component

To utilise the five constructed components required the quantification of I vs. V_s per component such that the peak-current ranges could be defined. Furthermore, it was important that the desired peak-current set-point could be achieved by setting V_s, as only one attempt was permissible, given the limited availability of virgin gap sets purchased from Strike Technologies. Additionally, gap etching repeatability would otherwise be adversely affected for two groups of G = 2 and four groups of G = 1 per desired I set-point (refer to Chapter 3).

From equation (3.1), for a particular component under short-circuit conditions, varying V_s will vary I as follows:

$$I = \frac{C_c}{T_{Wg}} V_s \tag{5.1}$$

where I is the peak current (A), V_s is the (dc) generator voltage (V) and C_c is the capacitance (μF) for the particular capacitor configuration. T_{Wg} is defined as the area under the normalised current waveform in units of time (μs) i.e. an equivalent (square-pulse) duration for the generator that is unique for a particular waveform (refer to Chapter 3).

[1] The third component yields a 16/36 μs waveform, which lies beyond the "Area of interest" i.e. unsuitable for the creation of a benchmark sample; the sixth component yields a 5/72 μs waveform considered a reasonable approximation of a 4/70 μs waveform.

A thorough quantification over as much of the V_s range as was possible without over-stressing the solenoid-controlled spark gap, was conducted per component under short-circuit conditions (refer to Appendix F). Assuming that C_c remains constant over the V_s range, the T_{Wg} values were calculated.

The results show that the I vs. V_s relationship is almost 100% linear, whilst the variation in T_{Wg} is minimal (standard deviation around 1%) per component. Table 5.1 shows I / V_s and I_{max} according to the trend-line per component (refer to Appendix F), and calculated T_{Wg} per component. The T_{Wg} values show that the 5/72 μs waveform and 4/70 μs waveforms are very similar.

Table 5.1: I/V_s, I_{max} and T_{Wg} per component

COMP.	WAVE-FORM	I / V_s (kA/kV)	I_{max} (kA)	T_{Wg} (μs)
1	8/20 μs	0.6862	13.7	12.35
2	8/20 μs	2.6993	54.0	12.57
4	4/70 μs	0.0880	1.8	96.30
5	4/70 μs	0.3525	7.1	96.26
6	5/72 μs	1.0305	10.3	99.27

5.2 Defining the Peak-Current Ranges

Using the I vs. V_s relationships, the peak-current set-points per waveform using Components 1, 2, 4, 5 and 6 were defined to meet three criteria:

- Non-overlapping peak-current (I) ranges per waveform;
- Five evenly-spaced I set-points per component (refer to Chapter 3);
- I_{min} corresponding to $V_{s,min}$ = V_{so} = 2.5 kV to ensure spark-over for a single gap i.e. G = 1 (refer to Chapter 3).

Additionally, for gap etching repeatability it was determined (refer to Chapter 3) that each sample (waveform/peak-current set-point) must comprise four gaps, grouped as dictated by the V_s set-point relative to V_{so}, where each gap group would be subjected to a single impulse, as follows:

- $V_s \geq 10$ kV: one gap group of $G = 4$;
- 5 kV $\leq V_s <$ 10 kV: two gap groups of $G = 2$ (i.e. 2 + 2);
- 2.5 kV $\leq V_s <$ 5 kV: four gap groups of $G = 1$ (i.e. 1 + 1 + 1 + 1).

Figure 5.1 shows the test jig designed and built to hold one, two and four gaps in series. A longitudinal section was cut out of the conduit to reduce its inner diameter from 40 mm to 33 mm to ensure a snug fit for the gaps with the aid of elastic bands. Elastic bands (not shown) hooked around the perspex stirrups serve to compress the gaps together to ensure good electrical contact.

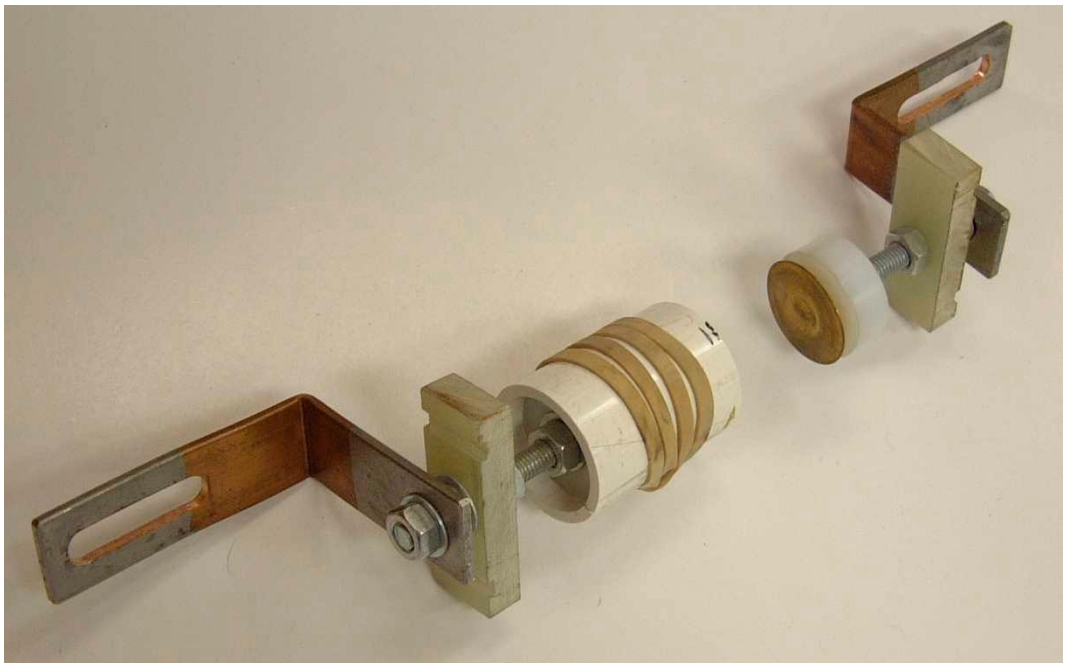

Figure 5.1: Test jig to hold surge arrester gap sets

5.3 The Reduced Benchmark Sample

Appendix G contains the completed reduced benchmark sample test sheet[2] representing 100 unique gap etching pairs. For each impulse application the current waveform was recorded (using 2500 points) yielding a total of 40 recorded[3] waveforms – the waveform filenames are listed. The desired peak-current set-points were achieved with minimal error, indicating that loading of the generator by the test piece is negligible.

[2] The sample number sequence reflects omission of the 4/40 μs and 4/55 μs waveforms.
[3] One recording was accidentally omitted.

Upon removal of the gaps from the test jig, the polarity of each gap plate was marked as either positive (anode) or negative (cathode) as referenced to the lightning impulse generator DUT terminals.

5.3.1 Select gap etching examples

Figures 5.2 to 5.6 show select examples of gap plate pairs with etchings for each of the waveforms.



Figure 5.2: Gap etchings for 7.4 kA, 8/20 μs waveform (sample 3)



Figure 5.3: Gap etchings for 52.6 kA, 8/20 μs waveform (sample 10)



Figure 5.4: Gap etchings for 0.4 kA, 4/70 μs waveform (sample 46)



Figure 5.5: Gap etchings for 2.0 kA, 4/70 μs waveform (sample 51)



Figure 5.6: Gap etchings for 7.0 kA, 5/72 μs waveform (sample 56)

5.3.2 Preliminary visual inspection

In view of the aim of this work viz. to create a benchmark sample such that field-gap etchings may be categorised according to the closest visual match, preliminary visual inspection of the 100 gaps (i.e. 200 gap plates) was conducted, yielding the following observations:

- The larger etchings are mostly ellipsoid; the smallest are often irregular;
- In a few rare cases, an etching comprises a grouping of two or three ellipsoid etchings, which may overlap;
- For the bipolar (8/20 μs) waveform, the etchings on a pair of gap plates are virtually identical i.e. dull molten area;
- For the unipolar waveforms (4/70 μs and 5/72 μs), the etchings are distinctly different i.e. shiny molten area for the positive gap plate (or anode) vs. dull molten area for the negative gap plate (or cathode) - geometrically the gap plates are identical;
- The largest etchings are not confined to the central hub area – in extreme cases gap material vapourised and settled on the plates as a black (possibly oxide) deposit. The black deposit density increases with increasing current.

Therefore apart from the size of the etching, additional information is the appearance of the etching (dull vs. shiny) yielding the polarity of the surge, or indicating that the surge is bipolar. In cases where the etching is not confined to the central hub area, the density of the black deposit possibly yields a secondary level of categorisation in terms of peak-current magnitude.

5.4 Measurement of Gap Etching Area

Although the original aim of the benchmark sample was to facilitate the categorisation of field-gap etchings according to the closest visual match, further analysis allows the relationship between gap etching area and peak current to be explored through measurement and analysis of the benchmark sample etchings.

Measurement of the gap etching area also allows a more scientific basis for the assessment of repeatability, otherwise performed on a purely visual basis.

5.4.1 Ellipsoid approximation

Ideally the gap etchings could be digitally scanned and the area of each gap etching measured using suitable software. Some exploratory work utilised a flat-bed scanner, but the resolution was poor (especially for the small etchings) and the gap etching images were distorted by light reflection off the gap plates. Furthermore it was clear that manual intervention would be necessary to define the measurement area to the software application, indicating a very lengthy process to categorise 200 gap etching plates.

During the course of the above-mentioned exploratory work, a number of etchings were inspected using a Nikon V-12 Profile Projector with 20x- and 50x-magnification with a measurement system allowing x-y measurements to an accuracy of 1 micron. Given that most gap etchings are ellipsoidal, an etching area may be approximated by:

$$A_e = \frac{\pi}{4} D d \tag{5.2}$$

where D and d are the major and minor axis diameters (mm) respectively derived from the measured Cartesian co-ordinates (refer to Figure 5.7).

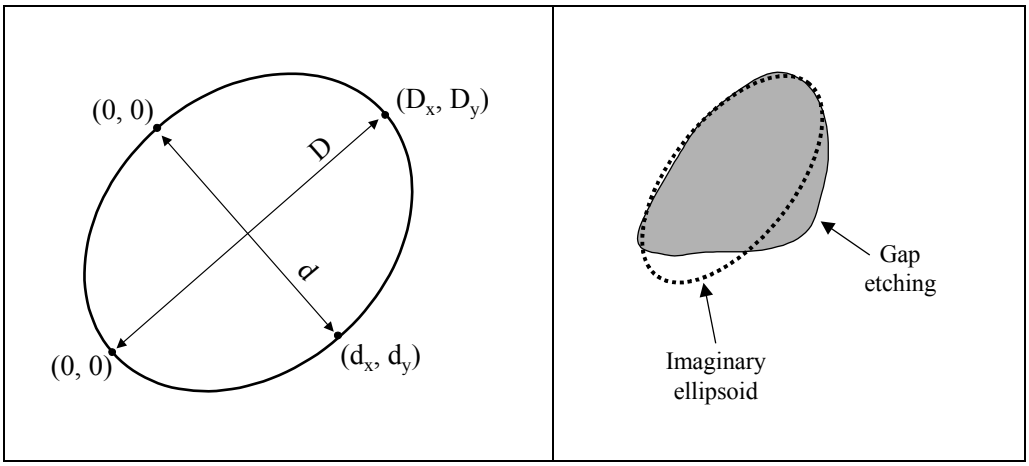

Figure 5.7: Ellipsoid Cartesian co-ordinates; imaginary ellipsoid approximation

For distinct multiple etchings, measurements are separately made, whilst for the irregularly shaped and overlapping etchings, some imagination is required i.e. by mentally shifting etching area to form an ellipsoid (refer to Figure 5.7). The potential for errors incurred in employing the ellipsoidal approximation, especially with regard to the imaginary ellipsoid, is considered minimal because up to eight gap etchings contribute to each mean gap etching area value.

5.4.2 Gap etching area measurement guideline

During measurement, two interrelated obstacles were encountered:

- Profile projector: The object is illuminated via a beam of light directed down through the lens system. The light is reflected from the object back through the lens system, and projected onto an opaque screen. A distinct disadvantage is that any sloped or matte area scatters the light, thereby appearing as a black or dark area on the screen, and resulting in measurement confusion;

- Unipolar (4/70 μs and 5/72 μs) waveforms: For peak impulse current less than 6 kA, the negative gap plate (or cathode) etching area is larger than the positive gap plate (or anode) etching area.

For the latter, careful scrutiny of the gap etchings using a 10x-magnification loupe showed that:

a) The molten area on the negative gap plate is smaller than that of the positive gap plate;
b) The molten area on the negative gap plate is surrounded by a matte area without a clearly defined border – this is not apparent to the naked eye – rendering the negative gap plate etching larger than the positive gap plate etching;
c) For larger peak impulse current, a black border defines the matte area and the gap etching areas are essentially the same size.

Similarly careful scrutiny of the gap etchings for the bipolar (8/20 µs) waveform also showed matte areas with and without defined borders, but for these gaps the etchings are identical per pair of gap plates.

These findings prompted the compilation of a visual gap etching measurement guideline (refer to Figure 5.8), which shows that any gap etching comprising a matte area without a clearly defined border must be ignored.

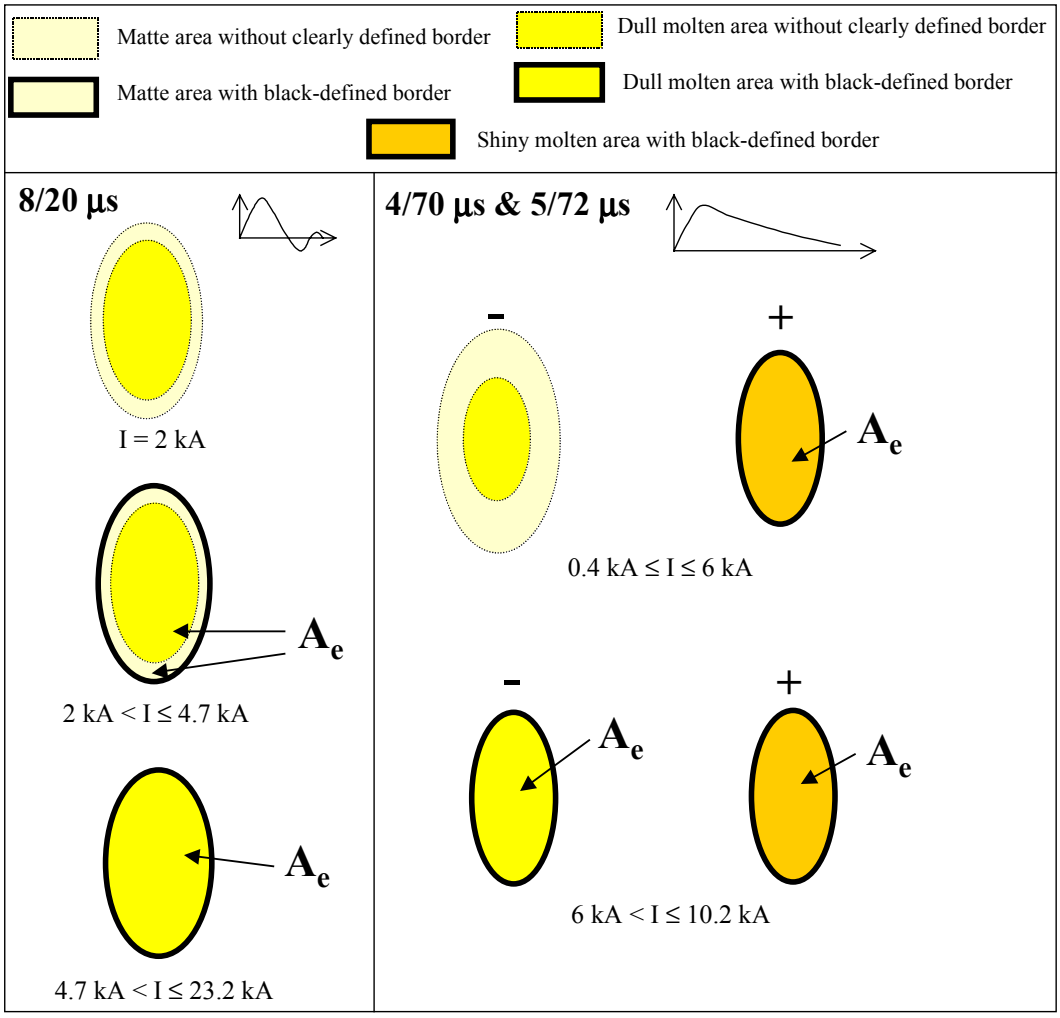

Figure 5.8: Visual gap etching area measurement guideline

Therefore prior to actual measurement using the profile projector, each gap etching was first studied using the 10x-magnification loupe. The measurement guideline also shows that for unipolar waveforms it is possible to deduce the direction of lightning impulse current flow through a gapped surge arrester i.e.

dull molten area vs. shiny molten area for negative and positive gap plate respectively.

The gap etching measurement data is contained in Appendix H, which includes the calculated gap etching area per gap plate, as well as the mean and standard deviation for the available data. As is evident in the data, the gap etchings for the 2 kA, 8/20 μs gap plates were not particularly measurable as per the measurement guideline.

5.5 Gap Etching Area Analysis

Plots of A_e vs. I per waveform are shown in Figure 5.9, where the relationships appear to be approximately linear for the 4/70 μs and 5/72 μs waveforms, and initially linear for the 8/20 μs waveform.

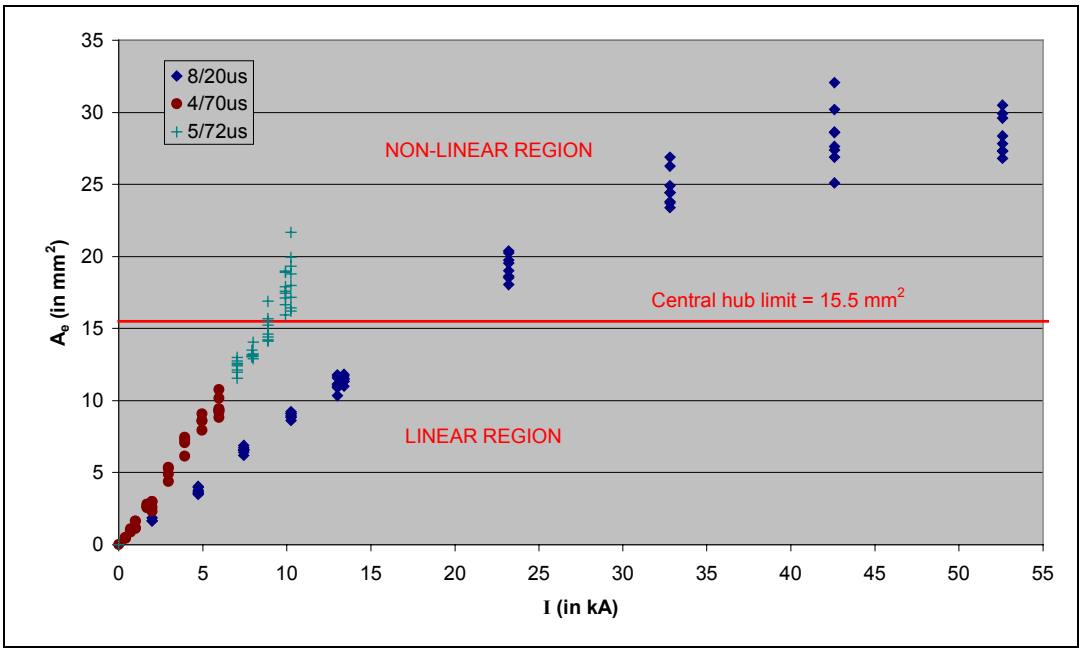

Figure 5.9: A_e vs. I per waveform

5.5.1 Central hub limit

Inspection of the benchmark sample shows that these linear relationships hold whilst the gap etching is constrained to the central hub area of the gap plate.

The central hubs of a gap plate pair are parallel, forming the spark gap (refer to Figure 5.4) – beyond the central hub, the gap plate material tapers away (initially slowly) i.e. increasing gap size.

The central hub area is on average 15.5 mm^2 (refer to Figure 5.9) based on the measurement of eight virgin gap plates, and therefore provides a limit to the linear region of A_e.

5.5.2 Gap etching area statistical spread

Figure 5.10 shows the standard deviation as a percentage of the mean gap etching area for each waveform/peak-current combination.

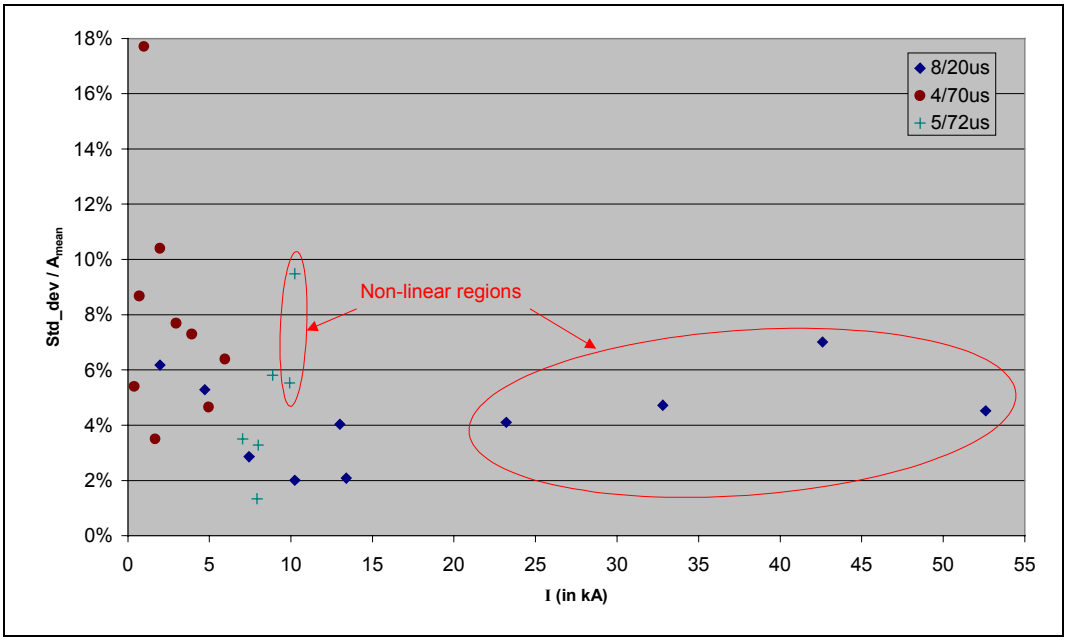

Figure 5.10: Standard deviation as a percentage of mean gap etching area

Standard deviation less than 10% of the mean etching area is deemed sufficient to demonstrate good etching repeatability (refer to Chapter 3). This was achieved for all the waveform/peak-current combinations, excepting: 4/70 μs, 1 kA (> 17%) and 4/70 μs, 2 kA (> 10%), where the low peak-current yields irregularly-shaped etchings, and hence higher risk of measurement error. Variation in the gap size due to gap plate manufacturing inconsistency is a possible source of error.

For I < 15 kA, the standard deviation as a percentage of the mean gap etching area decreases with increasing peak-current, but increases slowly for I > 15 kA. In the former, the gap etching areas become increasingly better defined i.e. from irregularly-shaped to ellipsoidal; in the latter, the gap etching areas increasingly extend beyond the central hub area.

5.5.3 Dependency of A_e on I per waveform

Ignoring all (except marginal) data in the non-linear regions, the dependency of A_e on I for the three waveforms is shown in Figure 5.11.

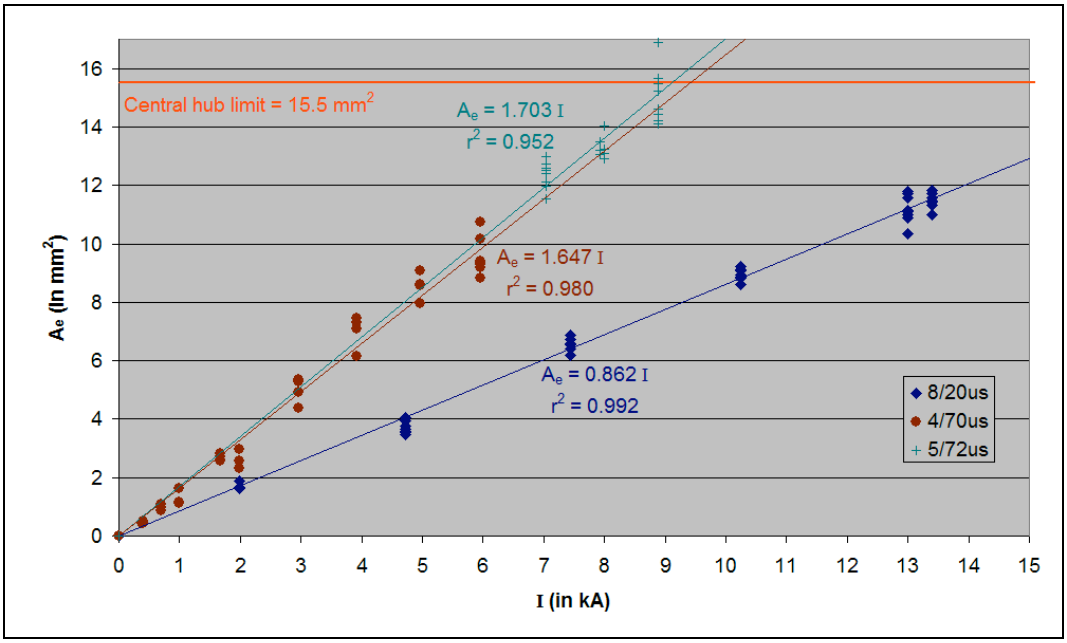

Figure 5.11: A_e vs. I per waveform – censored data

For each waveform, the trend-line - with associated coefficient of determination (r^2) - shows that the A_e vs. I relationship is linear within the central hub area. As expected, the trend-line for the 5/72 μs waveform lies very close to that of the 4/70 μs waveform; combining the data for these two waveforms yields A_e = 1.689 I with r^2 = 0.988. Therefore the following empirical equations hold per waveform:

$$A_e = 0.862 \times 10^{-3} I \qquad \text{(8/20 μs)} \qquad (5.3)$$

$$A_e = 1.689 \times 10^{-3} I \qquad \text{(4/70 μs)} \qquad (5.4)$$

where A_e is gap etching area (mm^2) and I is peak impulse current (A).

Given the existence of empirical expressions for A_e vs. I for the 8/20 μs and 4/70 μs waveforms, the area of a field-gap etching may simply be measured and the associated peak current calculated for each waveform, provided the etching does not extend beyond the central hub. Indeed, subsequent to the creation of the benchmark sample and as part of his Eskom duties, the author (Koert, 2003) analysed a sample of 672 field-gaps from Eskom's Central Region. This region has the highest ground flash density (N_g = 7 flashes/km^2/year) out of the seven Eskom Regions covering South Africa. The measured etchings, representing a service life ranging between 0 and 9 years (average service life of 4.05 years), were all well confined to the central hub.

5.5.4 Benchmark sample – further considerations

Due to time constraints, the 4/40 μs and 4/55 μs waveforms were excluded in the creation of the benchmark sample – hence the reduced benchmark sample. Nevertheless it is expected that the A_e vs. I curves for these waveforms will also be linear for etchings confined to the central hub. Furthermore, it is expected that these curves will lie between those of the 8/20 μs and 4/70 μs waveforms, where the longer the waveform duration, the steeper the curve gradient, suggesting a combined curve of the following form:

$$A_e = k\, I\, T_W^y \qquad (5.5)$$

where k is a constant of proportionality (mm^2/A.s^y), I is peak impulse current (A), y > 0, and T_W is the equivalent duration (s) for the particular waveform defined as follows (refer to Chapter 2):

$$T_W = \int_0^T \left| \frac{i(t)}{I} \right| dt \tag{5.6}$$

i.e. the area under the normalised (absolute) current waveform, where T is the waveform duration (s).

Using the waveform parameters given in Chapter 3 (refer to Table 3.1) to construct the waveforms and setting T to a large value (e.g. 5000 μs), T_W evaluates to 23.2 μs and 94.9 μs for the 8/20 μs and 4/70 μs waveforms respectively. Then, first combining equations (5.5) and (5.3), and then equations (5.5) and (5.4), yields the following two equations:

$$k\left(23.2\times10^{-6}\right)^y = 0.862\times10^{-3} \tag{5.7}$$

$$k\left(94.9\times10^{-6}\right)^y = 1.689\times10^{-3} \tag{5.8}$$

Dividing equation (5.8) by equation (5.7), solving for y and then solving for k yields equation (5.5) as follows:

$$A_e = 0.141\, I\, T_W^{0.477} \tag{5.9}$$

Using the waveform parameters given in Chapter 3 (refer to Table 3.1) to construct the waveforms and setting T to a large value (e.g. 5000 μs), T_W evaluates to 51.5 μs and 72.5 μs for the 4/40 μs and 4/55 μs waveforms respectively. Substituting these values in equation (5.9) yields the following estimated equations:

$$A_e = 1.270\times10^{-3}\, I \qquad \text{(4/40 μs)} \tag{5.10}$$

$$A_e = 1.495\times10^{-3}\, I \qquad \text{(4/55 μs)} \tag{5.11}$$

where A_e is gap etching area (mm^2) and I is peak impulse current (A).

It must be noted that this is by no means a rigorous treatment, as it has not been established that T_W is the appropriate parameter in equation (5.9). This equation

can only be verified using a third empirical curve based on a significantly different waveform to the 8/20 μs and 4/70 μs waveforms, and hence equations (5.10) and (5.11) must be treated with circumspection.

5.6 Conclusion

The peak-current range for each of the five usable constructed components was defined by quantifying I vs. V_s under short-circuit conditions. Furthermore this quantification allowed the desired I to be achieved almost precisely due to negligible loading by the test-piece, even for $G = 4$, thereby ensuring repeatability.

Due to time constraints the resulting reduced benchmark sample partially fulfils the original aim of this work i.e. only the 4/70 μs waveform, as per "Area of interest" (refer to Figure 2.2), is represented. However the 8/20 μs (industry standard) waveform is additionally represented.

The original aim of the benchmark sample was to facilitate the categorisation of field-gap etchings according to the closest visual match. Apart from the size of the etching, preliminary visual inspection of the benchmark gap etchings revealed additional information relating to the polarity of unipolar surges; for bipolar surges the appearances of the etchings is the same for the gap plate pair. Furthermore, a secondary level of peak-current categorisation may exist in cases where the etching is not confined to the central hub.

However given that most of the gap etchings are ellipsoidal (or may be approximated by an imaginary ellipsoid), an empirical linear relationship between gap etching area and peak current emerged per waveform, once all gap etching areas - constrained to the central hub area of the gap plate - had been measured. As would be expected, the physical extent of the central hub provides a limit beyond which these relationships are no longer linear because the gap size increases. The major and minor axis diameters were measured using a profile projector with 20x- and 50x-magnification and with a measurement system allowing x-y measurements to an accuracy of 1 micron. The etchings are not always clearly defined with the possibility of measurement error due to the nature

of operation of the profile projector; this prompted the compilation of a visual gap etching measurement guideline, where each etching is first inspected using a 10x-magnification loupe. Overall, the standard deviation of the gap etching areas for most of the waveform/peak-current combinations is less than 10%, indicating that the ellipsoid approximation and human measurement error are acceptable.

The A_e vs. I empirical expressions for the 8/20 μs and 4/70 μs waveforms enable the calculation of peak currents for a measured field-gap etching area, provided the etching does not extend beyond the central hub. The author's subsequent analysis of a sample of 672 field-gaps from Eskom's Central Region, has shown that it is unlikely that etchings will extend beyond the central hub.

The estimated A_e vs. I expressions for the 4/40 μs and 4/55 μs waveforms must be treated with circumspection, as they are computed from the available data for the 8/20 μs and 4/70 μs waveforms. Ideally a third empirical curve based on a significantly different waveform to the 8/20 μs and 4/70 μs waveforms, is required to verify these expressions.